Development of a Mesoscale Inversion System for Estimating Continental-Scale CO2 Fluxes

Daniel Wesloh, Thomas Lauvaux, Kenneth J. Davis

JAMES | Journal of Advances in Modeling Earth Systems

RESEARCH ARTICLE
10.1029/2019MS001818

Special Section:
Carbon and Weather: Results from the Atmospheric Carbon and Transport – America Mission

Development of a Mesoscale Inversion System for Estimating Continental-Scale CO_2 Fluxes

Daniel Wesloh[1], Thomas Lauvaux[1,2], and Kenneth J. Davis[1,3]

[1]Department of Meteorology and Atmospheric Science, The Pennsylvania State University, University Park, PA, USA, [2]Laboratoire des Sciences du Climat et de l'Environnement, Gif sur Yvette, France, [3]Earth and Environmental Systems Institute, The Pennsylvania State University, University Park, PA, USA

Abstract Computational requirements often impose limitations on the spatial and temporal resolutions of atmospheric CO_2 inversions, increasing aggregation and representation errors. This study enables higher spatial and temporal resolution inversions with spatial and temporal error structures similar to those used in other published inversions by representing the prior flux error covariances as a Kronecker product of spatial and temporal covariances and by using spectral methods for the spatial correlations. Compared to existing inversion systems that are forced to degrade the resolution of the problem in order to bring the dimensionality down to computationally tractable levels, this inversion framework is able to take advantage of mesoscale transport simulations and more of the complexity of spatial and temporal covariances in the surface CO_2 fluxes. This approach was successfully implemented over one month with an identical-twin observing system simulation experiment (OSSE) using a set of assumptions about the prior flux uncertainties compatible both with continental-scale uncertainty estimates and with comparisons of vegetation models to flux towers. The demonstration illustrates the potential of the newly developed inversion system to use high-temporal-resolution information from the North American tower network, to extract high-resolution information about CO_2 fluxes that is inaccessible to coarser resolution inversion systems, and to simultaneously optimize an ensemble of prior estimates. This demonstration sets the stage for regional flux inversions that can take full advantage of the high-resolution data available in tower CO_2 records and mesoscale atmospheric transport reanalyses, include more realistic prior error structures, and explore specifying prior fluxes with ensembles.

Plain Language Summary This paper describes a new inverse framework for deriving surface carbon dioxide (CO_2) fluxes at high spatial and temporal resolutions from atmospheric mole fraction measurements. We demonstrate the potential of the system over North America by inverting for subdaily biogenic CO_2 fluxes while accounting for the complexity of spatio-temporal structures in flux error covariances in a data-based manner.

Key Points:
- A new inversion system uses spectral methods for spatial correlations to do a 27 km subdaily inversion over North America
- The software package allows simultaneous optimization of multiple prior mean flux estimates
- The system is demonstrated over continental North America for a network of seven towers

Supporting Information:
- Supporting Information S1

Correspondence to:
D. Wesloh,
dfw5129@psu.edu

Citation:
Wesloh, D., Lauvaux, T., & Davis, K. J. (2020). Development of a mesoscale inversion system for estimating continental-scale CO_2 fluxes. *Journal of Advances in Modeling Earth Systems*, *12*, e2019MS001818. https://doi.org/10.1029/2019MS001818

Received 17 JUL 2019
Accepted 17 JUL 2020
Accepted article online 21 JUL 2020

1. Introduction

The global atmospheric carbon dioxide (CO_2) concentration has been steadily increasing since the first industrial revolution; the current rate is equivalent to a net positive flux to the atmosphere of about 4.7 ± 0.1 PgC/yr over the last decade (Le Quéré et al., 2018). Emissions from fossil fuel consumption, the main driver of this increase, reached 9.4 ± 0.5 PgC/yr over this same decade (Andres et al., 2014; Le Quéré et al., 2018).

Tans et al. (1990) shows that half of the CO_2 emitted from anthropogenic activities, instead of staying in the atmosphere, is being absorbed by the oceans and by continental vegetation, with each responsible for roughly half of the uptake (Battle et al., 2000). As fossil fuel emissions have grown, atmospheric accumulation has remained fairly constant, showing that the uptake has increased at a similar pace (Le Quéré et al., 2016). Our understanding of the underlying processes driving the uptake of CO_2, especially over continental surfaces, remains limited (Ryu et al., 2019). This limits our ability to predict future changes in CO_2 mole fractions (Friedlingstein et al., 2014; Huntzinger et al., 2017; Schimel et al., 2015) and their impact on Earth's climate.

Several methods exist for estimating the carbon uptake by land ecosystems. One common approach is to inventory vegetation biomass reservoirs every few years (Hayes et al., 2012; Pacala et al., 2001). While direct and powerful, this approach is labor intensive, has low temporal resolution, does not measure lateral transport, may not fully account for new forests (Houghton et al., 2012), and at present undersamples the tropics

and high latitudes (Anav et al., 2015; Zhao et al., 2006). In addition, soil carbon stocks are not typically included in biomass inventory measurements.

Another approach uses terrestrial biogeochemical models able to simulate the processes of photosynthesis, respiration, and decomposition. This approach enables a more mechanistic understanding of the carbon cycle, complementary to biomass inventory data. How these processes are represented varies among models (Table 1, Anav et al., 2015; Schwalm et al., 2010). Uncertainties in the representation of ecosystem-level processes (Wessman, 1992) and uncertainties in the model inputs lead to large differences in carbon fluxes among terrestrial biosphere models (Huntzinger et al., 2012; King et al., 2015; Schwalm et al., 2010). However, these differences between models are not large enough to include eddy covariance estimates of the fluxes within the envelope of model-derived estimates of the same fluxes (Anav et al., 2015; King et al., 2015; Normile & Davis, 2017; Raczka et al., 2013).

A third approach is to quantify CO_2 surface fluxes by combining atmospheric mole fractions of CO_2 with a priori information about spatially and temporally resolved estimates of biospheric, oceanic, and anthropogenic surface CO_2 fluxes in an atmospheric inversion. The assumptions made for a particular atmospheric inversion—whether about the transport of air from fluxes to observations (Díaz-Isaac et al., 2014, 2018; Gurney et al., 2002; Lauvaux & Davis, 2014; Peylin et al., 2002; Schuh et al., 2013; Seibert & Frank, 2004) or the a priori flux information itself (Gurney et al., 2003; Lauvaux, Schuh, Uliasz, et al., 2012; Peylin et al., 2013)—affect the results obtained. Despite increases in model resolution and atmospheric data density that have produced convergence in the annual mean between atmospheric top-down inversion methods and the bottom-up methods mentioned in previous paragraphs (Jacobson & Miller, 2018; Schuh et al., 2013; Ogle et al., 2015), inversion studies still often disagree in the spatial and temporal attribution of the CO_2 surface flux variability (Jacobson & Miller, 2018; Peylin et al., 2013).

Inversion methods combine a priori flux estimates with atmospheric measurements, both accompanied by estimates of their uncertainties, to form a better estimate of the surface CO_2 fluxes using Bayes's theorem (Barnard & Bayes, 1958; Bousquet et al., 2000; Ciais et al., 2010; Tarantola, 2005). As inversions are often used to solve for large-dimensional flux vectors using only a few atmospheric measurements, the problem is inherently ill-posed (Bocquet, 2005; Tarantola, 2005), requiring the addition of a priori estimates of the mean flux and its uncertainty to bring the number of data points used to constrain the system back above the number of unknowns (Enting & Mansbridge, 1989; Tarantola, 2005). These studies used large ecoregions or coarse grids with the assumption that fluxes were uncorrelated between regions and perfectly correlated within them to reduce the size of the problem; these wide-reaching correlations are inconsistent with observations (Chevallier et al., 2006; Lauvaux, Schuh, Bocquet, et al., 2012; Wu et al., 2013). In addition, Kaminski et al. (2001) and Law et al. (2002) note that if the source is spatially heterogeneous over such a region and the measurements are influenced much more by one part than by the others, this can significantly bias the results.

The primary difficulty in continental-scale inversions at mesoscale resolutions lies in representing the uncertainty as a covariance matrix. One approach to reduce the size of this matrix, mentioned above, is to assume that errors in the fluxes are perfectly correlated within large regions and uncorrelated between them (Gurney et al., 2002, 2003; Peters et al., 2007). Given these assumptions, all values off the main diagonal of the a priori uncertainty matrix are zero and no storage need be allocated for them. Another method, which does not require the specification of regions in advance, instead uses empirical orthogonal functions (Hotelling, 1933; Lorenz, 1956; Pearson, 1901) to represent the fluxes, which again allows the covariance to be made diagonal (Zhuravlev et al., 2011, 2013). Ray et al. (2013) presents another method for reducing the memory and computational requirements for an inversion: use a wavelet transform (Daubechies, 1988; Mallat, 1989; Torrence & Compo, 1998) to decorrelate the fluxes, thereby changing to a basis where the covariance is again diagonal (Ray et al., 2014, 2015). A contrasting method, Yadav and Michalak (2013), assumes that the dependencies of the prior error correlations on time and space were separable and showed that this assumption allows a reduction in the memory and computational requirements of the inversion (Gourdji et al., 2012; Hu et al., 2019).

While the methods of Ray et al. (2013, 2014, 2015) are a promising avenue of investigation, those papers apply the method to anthropogenic carbon dioxide fluxes and do not suggest how to apply wavelet methods to the existing body of research on biogenic flux error correlations (e.g., Chevallier et al., 2006, 2012; Hilton et al., 2013; Kountouris et al., 2015). Given the result of Ray et al. (2013, 2015) that the assumed correlation

structure is more important to the quality of the final result than even the prior mean estimate, this study opted to use spectral methods (Dietrich & Newsam, 1993; Nowak et al., 2003) to represent the spatial correlations, which are much simpler to use with a specified correlation function (section 3.1), and the methods of Yadav and Michalak (2013) to produce the full spatio-temporal error correlation matrix.

Inversion systems able to more fully describe the spatio-temporal error structures, when combined with higher-resolution atmospheric models, enable us to use additional information content available within high-frequency, continental measurement systems (Law et al., 2002, 2003; Ogle et al., 2015; Patra et al., 2008; Schuh et al., 2013) and significantly increase our confidence in inversion results (Kaminski et al., 2001; Law et al., 2002, 2003; Schuh et al., 2013). Gourdji et al. (2012), Hu et al. (2019), Schuh et al. (2013), and Kountouris et al. (2018a, 2018b) make steps in this direction, with the first two solving for the daily cycle of a week at a time at 1° spatial resolution, the third at roughly weekly temporal resolution and 30 and 10 km spatial resolution, and the last two at 0.5° spatial resolution and 3-hourly temporal resolution. Higher-resolution atmospheric data can be complemented by a more rigorous description of the uncertainty in the prior mean fluxes to be optimized by the inversion.

Given the relative sparsity of atmospheric mole fraction measurements, many features of the prior are often retained in the posterior flux estimate, especially at smaller scales. Previous studies have accounted for the potential for bias due to this adherence to the prior by running the inversion multiple times with different vegetation models used as estimates for the prior mean and noting in what ways the posterior mean estimates agree and disagree with each other (Lauvaux et al., 2018b).

The posterior covariance, representing the uncertainty in the fluxes after the inversion, is a large matrix and computationally prohibitive to compute in full. Yadav and Michalak (2013) proposed calculating the posterior covariance at a lower resolution than the prior mean, as did Bennett (2002). Bocquet et al. (2011) and Bousserez and Henze (2018) proposed optimal methods to reduce resolution. Michalak et al. (2004) and Bousserez et al. (2015) approximate the posterior uncertainty by generating samples from the assumed distributions for the prior fluxes and the observations, performing a series of inversions using those samples, and treating the results of those inversions as samples from the posterior distribution for the fluxes. This study applies the approaches of both Yadav and Michalak (2013) and Michalak et al. (2004) in parallel to investigate the differences between the two. Bousserez et al. (2015) provides an earlier comparison of deterministic and stochastic low-rank approximations of the posterior covariance. Their deterministic approximation is based on a BFGS minimization rather than the coarse-resolution approximation of Bennett (2002) and Yadav and Michalak (2013), and it is the latter that is used here.

Most previous studies have used low spatial (Peters et al., 2007) or temporal (Gourdji et al., 2012; Hu et al., 2019; Lauvaux et al., 2012; Ray et al., 2014) resolution, unless limited in scope to a small region (Schuh et al., 2013), as a means to get around computational limitations on the inversion procedure. Even those studies using ensembles to explore the uncertainty (Bousserez et al., 2015; Lauvaux et al., 2012; Michalak et al., 2004) use only a few members due to those same computational limitations.

This paper presents a mesoscale inversion system able to assimilate high-frequency atmospheric CO_2 mole fraction measurements to optimize surface CO_2 fluxes at high spatial and temporal resolutions by combining the Kronecker product representation of Yadav and Michalak (2013) with the spatial correlation representation of Nowak et al. (2003) and Dietrich and Newsam (1993). The prior flux error covariance matrix is described temporally using separate hyperparameters for weekly and subdaily time scales, while using a spectral description of the spatial covariances in CO_2 fluxes. The algorithm used to solve the problem was chosen to allow the optimization of several estimates of the prior mean at once, assuming a single prior covariance and transport, requiring only slightly more resources than the optimization of a single prior mean estimate. While the individual parts of this framework have appeared separately elsewhere, the authors are aware of no other study applying all of these at once.

This software is similar to the CarbonTracker-Lagrange code (ESRL, 2017) maintained by the National Oceanic and Atmospheric Administration (NOAA) Global Monitoring Division (GMD) and used in Hu et al. (2019), which also provides a python implementation of Yadav and Michalak (2013) and can also avoid most of the work when performing a multiple inversions where only the prior mean estimates differ. CarbonTracker-Lagrange additionally applies sparse matrix methods to reduce the memory requirements.

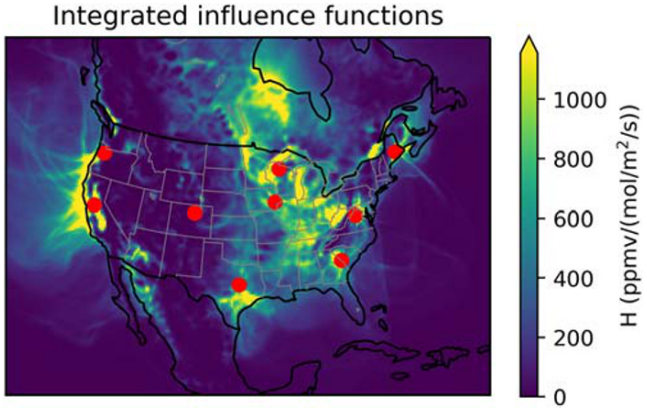

Figure 1. Model domain and tower locations for this study. The borders of the map are the edges of the WRF domain. The red circles denote tower locations. The background is influence functions summed over flux time and averaged over observations.

The inversion framework presented here is tested in a series of pseudo-data experiments over North America, demonstrating the potential of this approach to solve for subdaily surface CO_2 fluxes at 27 km resolution, similar to the resolution of the mesoscale atmospheric simulations used to drive the transport. The present framework is a step toward ensembles of multiyear inversions at subdaily temporal resolution with limited memory requirements.

2. Methods

The inversion framework described here combines a linearized adjoint model represented by explicit influence functions stored as a dense matrix, a priori surface fluxes, and continuous high-frequency atmospheric CO_2 mole fractions. Only the biogenic component of the surface flux is optimized in this inversion; extending this to estimate total surface flux in a real-data inversion would require a treatment of CO_2 inflow at the domain boundaries, but is otherwise straightforward.

2.1. Transport Adjoint Model

The adjoint model representing the physical relationship between the observation space (here atmospheric mole fractions) and the state space (here surface fluxes) is computed using the Lagrangian Particle Dispersion Model (LPDM) of Uliasz (1993, 1994). To produce this relationship, LPDM releases mass-free particles backward in time from the location of each observation and tracks them for up to 3 weeks or until they exit the domain. The configuration used in this study releases 35 particles from each tower location during each 20-s time step, that is, about 6,300 particles for a single hourly observation. Once released, the particle motion is described by the mean horizontal and vertical winds, the potential temperature, and the turbulent kinetic energy (TKE) variables of the 27 km Weather Research and Forecast (WRF) simulation described in Butler et al. (2020). The turbulent motion in the atmospheric boundary layer (ABL) is represented by random vertical displacements to simulate convective conditions, following the Mellor-Yamada ABL scheme (Mellor & Yamada, 1982), calculating the Lagrangian time scale from the TKE fields (Chen, 2006; Uliasz, 1993, 1994). LPDM does not redistribute particles to account for subgrid-scale deep convection.

Positions of the particles are stored to disk every 20 min while the wind fields are updated every hour. The particle fields are then postprocessed to produce gridded influence functions for each observation time at each tower at 27 km resolution following Equation 13 in Seibert and Frank (2004). These influence functions describe the relationship between the flux at each surface grid cell and the mole fraction at the observation locations (i.e., LPDM particle release locations). Fluxes are aggregated over 6-hr periods to reduce memory requirements while still representing the diurnal cycle. Inspection of the influence functions indicates that most of the particles for a given observation time have left the domain by 2 weeks before release. The 3-week simulation window used here will track the particles until they reach the domain boundaries, which is critical for producing complete estimates of what portions of the surface impacted the observations.

Influence functions for nine selected tower locations (available from Wesloh & Lauvaux, 2019) are presented in Figure 1; a description of that network is given in section 2.5. The inversion provides the most potential for improvement where the fluxes have the greatest influence on the measurement towers. For this combination of month and tower network, much of the Rockies, Mexico, and southeastern Canada do not strongly influence the observations and so cannot be effectively constrained by the inversion. Most corrections in these regions will be due to correlations with corrections in regions better constrained by the tower network.

LPDM gridding software was written to keep computational demands low while postprocessing continental-scale simulations. Details on where to find this code are available in Appendix A.

LPDM has been used in multiple previous inversion studies (Lauvaux et al., 2012; Lauvaux & Davis, 2014; Lauvaux, Miles, et al., 2016; Schuh et al., 2013; Wu et al., 2013).

A recent comparison of WRF- and LPDM-calculated mole fractions is presented in Karion et al. (2019), an older comparison of Lagrangian dispersion models is presented in Potempski et al. (2008), and both

studies additionally compare both WRF and LPDM to observations. A similar comparison of WRF-calculated to LPDM-calculated mole fractions for the towers used in this study showed model-model agreement within a few ppm and good correlation when there were strong signals in the data.

2.2. Inversion Methodology

The inversion methodology presented here uses the Bayesian matrix formulation described in Bousquet et al. (2000) and Ciais et al. (2010), which is similar in many respects to the four-dimensional optimal interpolation described in Ide et al. (1997). The prior for the fluxes $\mathbf{x}$ is given by $\mathbf{x} \sim \mathcal{N}(\mathbf{x}_b, B)$, where $\mathbf{x}_b$ is our prior mean estimate of the flux, B is the uncertainty around that mean flux expressed as the prior covariance estimate, and $\mathcal{N}(\cdot, \cdot)$ is the multivariate normal distribution. We also generated pseudo-observations $\mathbf{y} \sim \mathcal{N}(H\mathbf{x}_b, R)$, where H is the transport operator (i.e., the influence functions presented in the previous section), and R describes the uncertainty in the instrument measurement procedure as well as in the transport mapping H. We can combine these using Bayes's theorem, producing a posterior flux estimate given by $\mathbf{x} \sim \mathcal{N}(\mathbf{x}_a, A)$, where

$$\mathbf{x}_a = \mathbf{x}_b + K(\mathbf{y} - H\mathbf{x}_b), \tag{1}$$

$$A = (I - KH)B, \text{ and} \tag{2}$$

$$K = BH^T(HBH^T + R)^{-1}. \tag{3}$$

A is the uncertainty in the final estimate expressed as the posterior covariance, and K denotes the Kalman gain.

2.3. Observing System Simulation Experiments

To demonstrate the capabilities of this system, a realistic inversion configuration was prepared as an identical-twin observing system simulation experiment (OSSE) (Errico & Privé, 2018), based on a priori fluxes for July from real-data inversions (here Carbon Monitoring System [CMS]-Flux developed at NASA; NASA Carbon Monitoring System, 2013) and transport from January.

A full OSSE is designed to simulate all components of a real inversion (Errico & Privé, 2018), including flux error, background or initial condition error, transport error, and observation error. One way to simulate realistic transport and flux errors is to use different models and driver data for the "truth" than for the prior for the inversion, preferably also using higher resolution for the "truth" runs. Obtaining quantitative results from an OSSE comparable to those obtained from a similar observing system experiment require an extensive validation process (Errico et al., 2013). An identical-twin OSSE does not simulate as many of the errors that would be seen in the real world or a full OSSE (Privé & Errico, 2013), thereby eliminating the time required for validation; in this case, it is assumed that the transport and background error covariance are known perfectly. This provides a best-case scenario to test whether a given inversion methodology could work with real data (e.g., Lorenc, 1988). This paper also performs a fraternal-twin OSSE; in this case, the assumed covariance structure is correct but the parameters are incorrect. Fraternal-twin experiments are useful for looking at the impact of the parameters changed between the generation of the prior and the inversion on the results of the OSSE. This study additionally uses the fraternal-twin OSSE to investigate the relationship between the uncertainty reported by the inversion in this scenario and the known magnitude of the difference between the posterior mean flux estimate and the "truth."

Fluxes from July 2010 are used to ensure a large biospheric signal. For a real-data inversion or a fully-validated OSSE, it is important to use the transport corresponding to the fluxes used to obtain sensible results. However, this study is a proof-of-concept intending to show the viability of an approach, and so the choice of using fluxes not matched to the transport is made on practical grounds due to the limited availability of LPDM influence functions. The results presented in this study should not be sensitive to this mismatch.

Noise structures with covariances described in section 2.4 were added to a "true" flux map to generate prior mean flux estimates. Similarly, noise structures with covariances described in section 2.6 were added to observations simulated using the "true" flux map to generate pseudo-observations. These perturbed flux maps and observations were used as the prior mean estimates and observations, respectively, for an inversion to show the potential of the newly developed inversion system; this is close to the procedure for

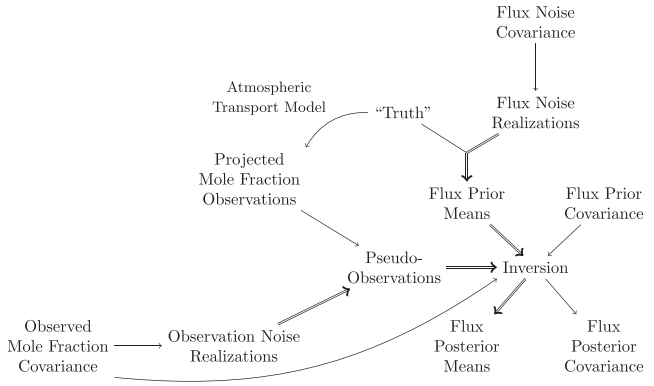

Figure 2. Flow chart describing the use of various variables for the experiments described in this section. Doubled lines denote parts with multiple realizations forming an ensemble. The noise realizations are the products of a pseudo-random number generator. The posterior means are generated from each pair of noisy observation and prior mean in turn. The "truth," noise, and noise covariance are unknown for real-data applications. The flux noise and prior covariances are identical for this experiment.

generating conditional realizations in Michalak et al. (2004); however, in this study, the same set of prior mean estimates are used for the identical- and fraternal-twin OSSEs to measure the effect of assumptions. We evaluate the ability of the inversion to recover the underlying, unperturbed "true" flux map for 80 noise realizations for both the prior and the observations. An overview of the various parts of the OSSE is given in Figure 2.

The a priori 4° × 5° biospheric surface CO_2 fluxes from the global CMS-Flux inversion system (Liu et al., 2014), developed at the NASA Jet Propulsion Laboratory and downscaled as described in Butler et al. (2020) were used as the "truth" for the OSSE.

2.4. Prior Uncertainties

Given the importance of the uncertainty estimates B and R to the final result, specifying them is an important step in any inversion (e.g., Wu et al., 2013): Many studies use multiple values for these parameters as a check on the robustness of their results (Gurney et al., 2003; Hu et al., 2019; Lauvaux et al., 2012). These are commonly given in terms of the variances and correlations of the deviations of the prior estimate from the truth. The relative magnitudes of the uncertainty estimates indicate how much one trusts the prior estimate compared to the information one can extract from the observations and reliably apply to specific fluxes.

2.4.1. Prior Flux Variances

In this pseudo-data inversion, prior flux variances at each point are assumed equal to a constant times the MsTMIP model-model mismatch (Fisher et al., 2016); these variances represent the uncertainty in the prior mean flux estimate for each point. These values are shown in Figure 3. This choice of variances allows for greater changes in the fluxes from prior to posterior in areas where vegetation models disagree while keeping areas where they agree closer to the prior mean estimate.

The constant factor multiplying the MsTMIP model-model variance, when combined with the assumptions about correlations from section 2.4.2 and aggregated to continental scales, should produce an uncertainty similar to those obtained for North America from other studies. A factor of 10 for the identical-twin experiment and 4 for the fraternal-twin experiment were determined to reproduce the Raczka et al. (2013) model-model differences for July reasonably well when used in combination with the correlations described in section 2.4.2, giving an uncertainty for the flux averaged over the whole spatio-temporal domain of 0.62 and 0.64 μmol/(m^{2}s), respectively, compared to 20 gC/(m^2 mo) = 0.6 μmol/(m^{2}s) from Raczka et al. (2013). Changing the correlations would require changing the constant factor to stay close to accepted values for the continental-scale uncertainty.

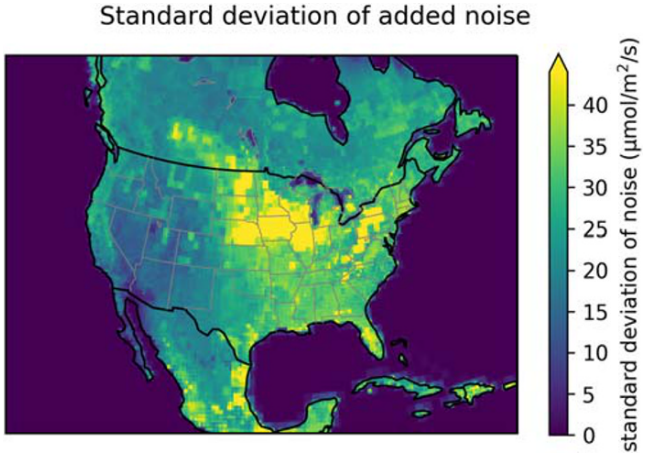

Figure 3. Ten times the standard deviation of the MsTMIP ensemble during July 2010, used as the standard deviation of the added noise and as the standard deviation assumed for the identical-twin inversion.

2.4.2. Prior Flux Correlations

We assume here that the correlations are the same at all points and in all directions, with specified functional forms for the correlations in space and time (for other examples, see Lauvaux et al., 2012; Wu et al., 2013; Yadav & Michalak, 2013). The functional forms require a length parameter, which describes the distance within which the correlations of required corrections are high, usually due to errors in plant type, soil properties, precipitation, radiation, and similar quantities being correlated over this distance. This method for specifying the correlations allows for greater flexibility in matching the observations than solving for large blocks (Ciais et al., 2010; Law et al., 2002; Schuh et al., 2013) as was done in, for example, Gurney et al. (2002, 2003) and Peters et al. (2007).

This paper assumes the spatial and temporal correlations are separable, that is, that the full prior spatio-temporal error correlation function is the product of a temporal correlation function and a spatial

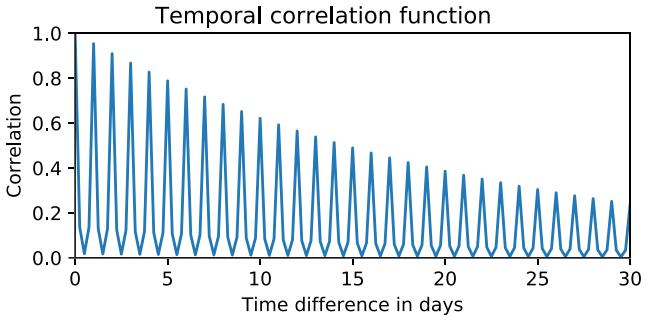

Figure 4. Temporal correlation function symmetric about zero lag. The corresponding correlations for other times can be obtained by shifting this one.

correlation function (for past examples, see Hu et al., 2019; Lauvaux et al., 2012). Some previous studies have found indications that the flux correlation length varies with time and the correlation function is therefore not separable (Huntzinger et al., 2011), but other studies on the subject have not found such evidence (Hilton et al., 2013; Kountouris et al., 2015). The assumption of separability allows the use of the methods of Yadav and Michalak (2013) to reduce the memory and time requirements for products of the full matrix with arbitrary vectors: The details of that calculation are described in the supporting information.

Since we assume the correlation functions depended only on distance and are independent of the location and orientation of the points, we can additionally make use of spectral methods in calculating and representing the spatial portion of the calculations. This representation of the correlations is described in greater detail in section 3.1. Past inversions have also accounted for shared plant types in the land cover (Lauvaux et al., 2012). Hilton et al. (2013) and Kountouris et al. (2015) do not support the usefulness of plant type in predicting correlations in the differences between a vegetation model and a flux tower at different locations, so the adjustment of correlations using plant types is not performed in this study.

The correlation function used in this paper is the exponential with length parameter r_0:

$$c(r; r_0) = e^{-r/r_0}, \tag{4}$$

as used in previous CO_2 flux inversion studies (e.g., Hu et al., 2019; Lauvaux et al., 2012). The length parameter r_0 is here taken to be 200 km, which is larger than the 100 km results from Chevallier et al. (2012), Wu et al. (2013), and Lauvaux et al. (2012) but smaller than the 400 km estimate obtained by Hilton et al. (2013) for annual fluxes from VPRM and on the low end of the 200 to 600 km range reported by Hu et al. (2019). The plots in Chevallier et al. (2006) do not allow a detailed comparison of correlation lengths beyond stating that there is no correlation at many hundreds of kilometers. Kountouris et al. (2015) suggests a correlation length of roughly 40 km for Europe but notes that the greater heterogeneity in Europe would likely decrease this value relative to similar values for North America. Since Hilton et al. (2013), Lauvaux et al. (2012), Wu et al. (2013), and Hu et al. (2019) focus on flux error structures in North America, this study placed more weight on those studies in the determination of the aforementioned 200 km correlation length.

This paper further splits the temporal correlation into two parts: the correlation between parts of the daily cycle and the correlation across days, with the overall correlation between two times defined as the product of these subcorrelations. Each part uses an exponential correlation function, the intradiel correlations with a time scale of 3 hours and the correlations between days with a time scale of 3 weeks; this is in contrast to Gourdji et al. (2012) and Hu et al. (2019), which assumed no correlations between parts of the daily cycle and a between-day correlation scale of 3 to 7 weeks. The correlations are plotted as a function of temporal separation in Figure 4. With this structure, the morning, afternoon, evening, and nighttime fluxes can vary somewhat independently of each other, but changes in any given time of day are closely tied to the changes in previous and subsequent days at the same time of day. This allows for the long correlation time scales suggested by Chevallier et al. (2006, 2012), Kountouris et al. (2015), and Hu et al. (2019) while acknowledging that photosynthesis and respiration are largely independent processes.

The alternate parameter values for the fraternal-twin OSSE are 1,000 km for the correlation length and 7 days for the correlation time.

2.5. Observation Network

This paper considers a network of pseudo-observations corresponding to permanent tall towers from the NOAA network. The GMD has deployed and maintained a network of eight towers over the last 15 years offering a continuous and high-accuracy measurement network to perform continental-scale inversions of greenhouse gases (Andrews et al., 2014). Seven of the eight towers were selected for our experiments covering different regions of North America: the Great Lakes (LEF), the upper Midwest (WBI), the southeastern

US (SCT), the southern Great Plains (WKT), New England (AMT), the mid-Atlantic (SNP), and the Rocky Mountains (BAO). The selected tower locations are marked by circles in Figure 1. These seven towers are enough to demonstrate the system and would be expanded to include more of the North American network of calibrated CO_2 mole fraction observations in a real-data inversion.

This study used only those observations that occurred between noon and 4 pm local solar time, when tower measurements are representative of the entire convective boundary layer (Bakwin et al., 1998; Davis et al., 2003) and modeling of the ABL is less uncertain (Agustí-Panareda et al., 2019; Chen et al., 2019; Geels et al., 2007).

2.6. Observation Error Covariances

The "observation error" covariance matrix R includes both the instrument error and errors in the representation of the influence functions H, that is, transport errors. The former tend to be independent for the hourly measurements used here (Andrews et al., 2014), while the latter tend to be correlated over several hours to a day and 1 to 400 km (Díaz Isaac et al., 2014; Lauvaux et al., 2009). This paper assumes towers are far enough apart to be uncorrelated in space, while temporal correlations in the transport errors fall off exponentially, with a 3-hr time scale.

Andrews et al. (2014) suggest values of 0.1 ppm for the uncertainty in the instrument readings. Gerbig et al. (2003; Figure 4) suggest 0.4 ppm is the approximate magnitude of errors of representativeness associated with comparing 27 km model grid-cell variables with point measurements. Lauvaux et al. (2009) suggest 2 ppm for the transport uncertainty based on a mesoscale ensemble, and Chen et al. (2019) suggest 3 ppm, while Díaz Isaac et al. (2014) imply values around 5 ppm might be more appropriate for this quantity.

This experiment assumes the standard deviation of the transport error for each observation to be 2 ppm in order to account for inaccuracies in the simulated atmospheric transport. The instrument errors and errors of representativeness are accounted for by means of an additional uncorrelated observation error covariance term with a standard deviation of 0.4 ppm. The pseudo-observations are calculated by finding the observations predicted by the influence functions using the "true" fluxes, then adding correlated noise with the characteristics described above.

2.7. Evaluation

Since this experiment is an OSSE, we can compute the error in the domain-average flux by subtracting the "true" flux from the prior and posterior mean estimates for each realization.

The setup of this experiment allows a comparison of two different measures of the uncertainty in the flux estimates: the analytic uncertainty from the calculated covariance matrices B and A and a Monte Carlo estimate from the spread among the individual mean estimates. For the identical-twin OSSE, these measures should be identical. For the fraternal-twin OSSE, these measures are expected to be different, with the difference indicating the degree to which the use of incorrect assumptions affects the uncertainty reported by the analytic approximation as compared to the expected model-"truth" discrepancy.

The analytic versions of B and A are stored at reduced resolution, and A is also calculated at reduced resolution, as discussed at the end of section 3. The Monte Carlo estimates of these matrices derived from the ensemble are subject to sampling error. Either of these sets of approximations may lead to disagreements between the analytic and Monte Carlo estimates of the covariance matrices.

To simplify presentation, these measures are shown only for the domain-average flux estimates.

3. Implementation

Spatial and temporal correlations at this relatively high resolution (27 km, producing a 184×249 spatial domain) required two main technical developments to efficiently represent and compute quantities using the background error correlation matrices: one class representing the Kronecker product representation of Yadav and Michalak (2013), described in the supporting information, and one providing a spectral representation of the spatial correlations as suggested by Nowak et al. (2003) and Dietrich and Newsam (1993) and as used in operational numerical weather prediction (Bannister, 2008), described in section 3.1.

These classes reduce the storage required for the background error covariance matrix from 330 TB to under 1 MB. The largest component left is then H. Since it is stored as a dense matrix, this inversion system is at present limited to about a month of observations. A description of how to get the code is available in Appendix A.

The above calculations consider only the requirements to produce an estimate of the posterior mean: Specifying the full posterior distribution requires also the posterior covariance. Storing the posterior covariance requires the same prohibitive amount of storage as the prior covariance, so approximations are needed. The method chosen here is to aggregate the fluxes to a coarser resolution in time and in space, specifically 7-day temporal resolution and 108 km spatial resolution and represent the covariances only on that reduced grid. Similar methods are suggested by Yadav and Michalak (2013) and Bennett (2002). The inversion package described in this paper provides functions to calculate reduction and prolongation operators able to modify the spatial parts of the background error covariance matrix B and observation operator H for lower spatial resolution but relies on the capabilities of the python package XArray for reducing the temporal resolution (Hoyer & Hamman, 2017) for ease of implementation and to avoid duplication of effort. The calculated reduction operator is a simple arithmetic mean within each of the coarser-resolution grid cells. The prolongation operator used here fills the whole of an averaged region with the average of that region.

The inversion functions in this framework can take the lower-resolution observation operator and background error covariance matrix as extra arguments and will use them to produce the posterior covariance estimate at the reduced resolution. The particular function used in this study uses the value of $HBH^T + R$ already calculated at full resolution while producing the posterior mean estimate, so that the full posterior covariance estimate is calculated as

$$A_{red} = B_{red} - B_{red}H_{red}^T(HBH^T + R)^{-1}H_{red}B_{red}, \tag{5}$$

rather than at full resolution as in Equation 2. The subscript *red* indicates that the subscripted quantity uses a coarse-resolution representation of the flux space, rather than the full-resolution representation of that same quantity used in the calculations for the posterior mean.

Note that the quality of the coarse-resolution inversion will depend on how much coarser its resolution is than the full resolution: Applying this method to find the covariance of the weekly fluxes averaged over the whole of the spatial domain will produce an invalid covariance matrix with entirely negative entries. In order to consistently have positive variance estimates available, this study calculated the posterior covariance twice, once without attempting to account for the aggregation error, using B_{red} and H_{red} directly in Equation 2:

$$A_{red,\,no\ agg} = B_{red} - B_{red}H_{red}^T(H_{red}B_{red}H_{red}^T + R)^{-1}H_{red}B_{red}, \tag{6}$$

which always produces a valid covariance. The quality of this second approximation for the posterior covariance will also depend on the resolution chosen. Several resolutions were chosen for the posterior covariance matrix, with the inversion run separately for each, saving both approximations each time, to provide information on how the posterior covariance matrix depends on resolution at which it is calculated and saved.

An effort was made during the development of this code to allow multiple prior mean estimates to be optimized at once, performing only a single calculation of $HBH^T + R$ and of the posterior covariance matrix A or A_{red} in the process; a similar procedure was proposed by Houtekamer et al. (1996) as a means to reduce the calculation required by an ensemble Kalman filter. Note that, when using this ability to approximate the posterior covariance using Monte Carlo methods following Michalak et al. (2004) and Bousserez et al. (2015), the quality of the approximation will depend on the number of realizations used.

3.1. Spectral Correlations

For correlations that are a function only of the distance between two points on a regular grid, the effect of the correlation is a convolution of the correlation with the fluxes, that is,

$$\sum_{i,j} F(x_j)C(x_j, y_i)F(y_i) \tag{7}$$

$$\sum_{j} F(x_j) \sum_{i} C(x_j - y_i)F(y_i). \tag{8}$$

This convolution can be represented in terms of the Fourier transforms of the correlation function $C(h)$ and the fluxes $F(x)$:

$$G(x) = \int_{\mathrm{y}} C(x-y)F(y)dy \;\Leftrightarrow\; \hat{G}(k) = \hat{C}(k)\hat{F}(k), \tag{9}$$

where the hat denotes the Fourier transform of the symbol (Equation 1.14.5 NIST Digital Library of Mathematical Functions, 2019). Using this approach, the correlation operator can be represented using only the spectral coefficients of the correlation function, which take up about the same space as the fluxes, and matrix-vector products can be calculated using the fast Fourier transform (FFT), which is much faster than the matrix multiplication (Cooley & Tukey, 1965; Gentleman & Sande, 1966; Stockham, 1966): The code for this paper uses the pyFFTW interface to the implementations in the Fastest Fourier Transform in the West (FFTW) library (Frigo & Johnson, 2005; Gomersall, 2016). This method uses the projected map coordinates to compute distances rather than using the proper great-circle distances. The assumption that the domain is doubly periodic in space, required by the FFT, is avoided by embedding the physical domain in a computational domain at least twice as large as the physical domain (Nowak et al., 2003). The elements of the computational domain that do not correspond to points in the underlying physical domain are set to zero, so that the correlations with those points do not affect the physical results.

Similar methods have been used in global meteorological data assimilation (Bannister, 2008), and a similar method was proposed by Nowak et al. (2003) for use in geostatistical problems. This is the first application the authors know of to the estimation of CO_2 flux inversions. Nowak and Litvinenko (2013) suggests combining spectral methods with methods for Kronecker products for further speedups, treating x and y as separable, in addition to space and time as is done here, and using a different algorithm for the Kronecker product.

4. Results and Discussion

Results for a single realization will be shown first, showing the structure implied by the prior covariance and the ability of the inversion to produce corrections to the daily cycle, followed by a summary of the 80 realizations together.

One realization of the noisy flux, that is, the true fluxes plus a perturbation generated with an exponential correlation function with this 200 km length scale, is shown in the second column of Figure 5 together with the "truth" from which it was generated in the first column. The estimate of the prior mean, shown in the middle column of Figure 5, does not look like the output of a modern vegetation model, with magnitudes much larger than expected and the sign varying widely across the domain. Since the prior covariance used to generate that prior mean estimate is intended to capture the spread of vegetation model outputs around the truth, the mismatch between the prior shown in Figure 5 and what would be expected from a vegetation model suggests that some of the assumptions going into the prior covariance are incorrect.

The changes from the prior to the posterior mean estimates in the two experiments are shown in the third and fourth columns of Figure 5. These changes appear smaller in magnitude than the prior mean estimate, indicating that the seven-tower network used here does not strongly constrain the gridpoint estimates. In addition, the smoothness of the changes indicates that the prior mean estimate is still relied upon for the fine-scale features. The changes in the fraternal-twin experiment are roughly the same magnitude but are smoother in space and change much more rapidly in time, showing the influence of the different parameters used in that experiment.

The average of the flux increment over the spatial domain for the first realization of the ensemble, that is, the change from the prior mean to the posterior mean, is shown in the middle plot in Figure 6. The high-frequency fluctuations in the blue line have a period of 1 day and show the inversion is able to adjust the daily cycle in addition to the larger-scale signals. Comparing the spatial average of the increment to the

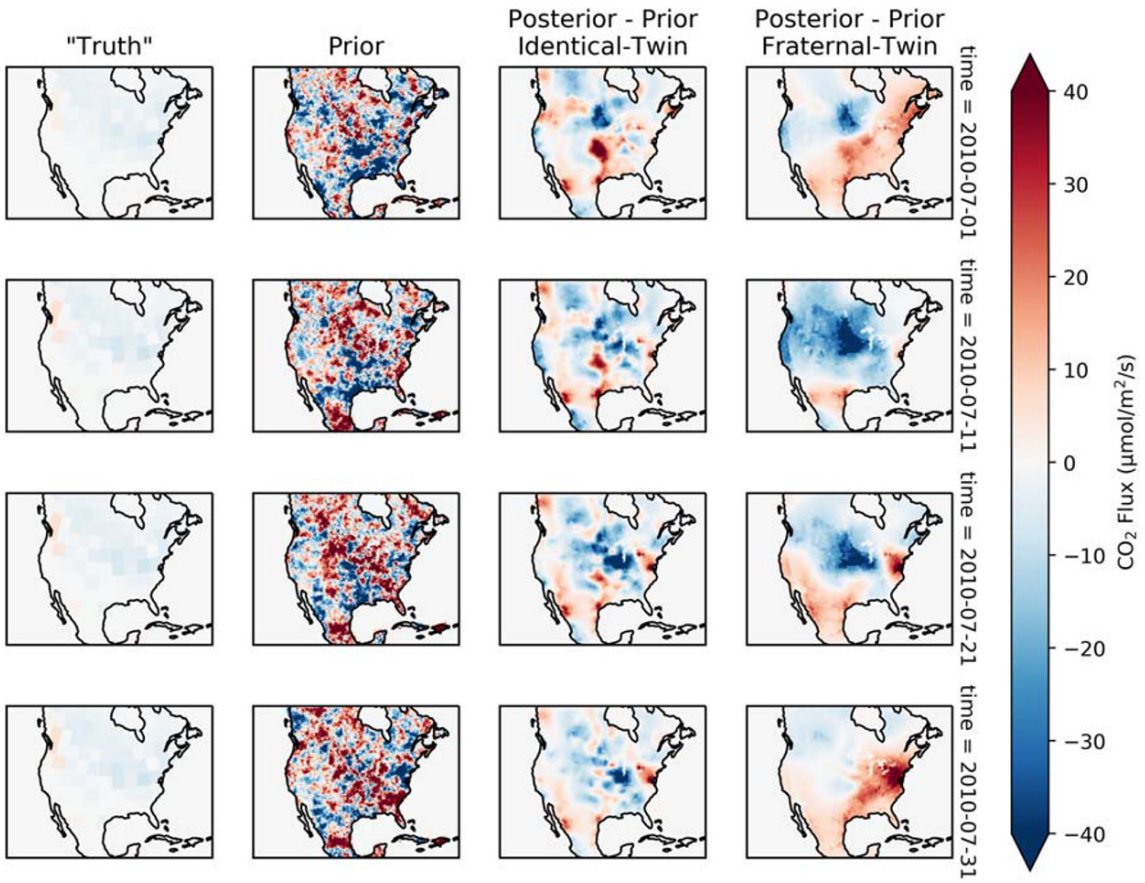

Figure 5. The left column shows the CMS posterior biological fluxes used as "truth" for these experiments. The second column shows a realization of the flux noise with an exponential spatial correlation function and a correlation length of 200 km, while the third column shows the mean of the posterior from the inversion performed with this prior mean estimate. The rows show the fluxes at different days, spaced 10 days apart, with each row showing the fluxes for midnight UTC.

spatial average of the prior and posterior mean estimates, shown in the top plot of Figure 6, indicates that the inversion improves both the net fluxes over several weeks and the magnitude of the daily cycle in those fluxes.

The bottom plot in Figure 6 shows the influence of the fluxes on the observations at any given time, represented as the sum of the influence functions corresponding to that flux time over the spatial domain and averaged over all observations. A larger influence means a given change in the fluxes can produce a larger change in mole fractions or, equivalently, that a given change in mole fractions would produce a relatively finer adjustment to the fluxes. All else equal, a larger influence allows for a larger change in the surface fluxes for a given observational mismatch.

The structure of the corrections shown in Figure 6 for the identical-twin experiment closely mirrors the temporal correlations shown in Figure 4: There are substantial variations within the daily cycle, but the variations from one day to the next are much smaller. By the same token, the fraternal-twin posterior changes much more from day to day, in accordance with the shorter correlation time scale. Both parts are exactly as allowed by the prior error correlations; this underscores the importance of the prior covariance in determining the output of the inversion and the need for data-driven error covariance structures.

The inversion of the 80 prior mean estimates was accomplished with a single run of the inversion code for each experiment, which shared the value of $HBH^T + R$ among the calculations required for the 80 posterior mean estimates and the reduced-resolution posterior covariance matrix. As a note, the updates to each prior mean estimate are independent of the other members of the ensemble. The posterior covariance matrix A_{red}

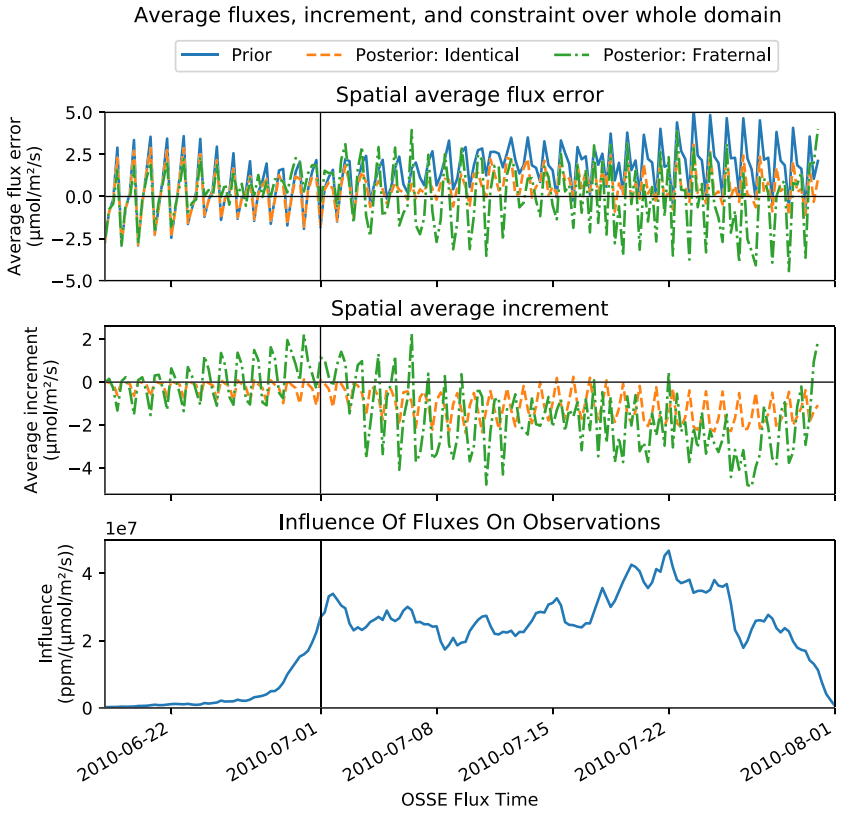

Figure 6. The top graph shows the magnitude of the difference between the prior and posterior estimates of the mean flux and the "true" flux the inversion was attempting to recover averaged over the spatial domain, both for the first ensemble member. The middle graph shows the change from the prior to the posterior mean flux estimates, again for the first ensemble member and averaged over the spatial domain. The bottom graph shows the influence of the fluxes at a given time on the average observation, also averaged over the spatial domain. The vertical line in each graph marks 1 July, the day of the first observation used in the inversion.

depends only on B, H, and R, and so is the same for all the realizations, and was only calculated twice: once with an attempt to account for aggregation error and once without. This demonstrates the potential for efficiently optimizing an ensemble of prior flux estimates. As with the assumptions concerning the temporal structure of the prior flux estimates, the creation of data-driven prior flux ensembles is a high priority for future research (Zhou et al., 2020).

In this inversion system, the ensemble of posterior fluxes can be used to estimate the uncertainty in the posterior fluxes in the manner of Michalak et al. (2004) and Bousserez et al. (2015). This system also allows for an approximate calculation of the analytic posterior uncertainty.

Table 1a
Standard Deviations for Domain-average Fluxes, in µmol/(m^2 s), Calculated Using Monte Carlo Methods

Monte Carlo									
	Prior			Identical-twin posterior			Fraternal-twin posterior		
N	Estimate	95 % CI		Estimate	95 % CI		Estimate	95% CI	
5 samples	0.90	0.43	2.05	0.53	0.22	1.22	0.53	0.25	1.22
10 samples	0.66	0.41	1.10	0.49	0.31	0.81	0.63	0.40	1.05
20 samples	0.61	0.45	0.86	0.37	0.27	0.52	0.51	0.37	0.72
40 samples	0.55	0.44	0.70	0.32	0.26	0.40	0.40	0.32	0.51
80 samples	0.62	0.53	0.72	0.30	0.26	0.36	0.38	0.33	0.45

Table 1b
Standard Deviations for Domain-average Fluxes, in μmol/(m^2 s), Calculated Using Two Different Deterministic Approaches. Missing Values Are Due to Negative Variances

Deterministic						
	Identical-twin experiment			Fraternal-twin experiment		
Resolution	Prior	Posterior (no agg.)	Posterior (attempt agg.)	Prior	Posterior (no agg.)	Posterior (attempt agg.)
108km	0.59	0.21	0.24	0.60	0.15	—
162km	0.59	0.20	0.20	0.60	0.15	—
216km	0.59	0.19	0.09	0.59	0.14	—
432km	0.58	0.18	—	0.59	0.14	—

Note. These standard deviations correspond to an uncertainty estimate for the average flux over the portion of the continent shown in Figure 1 and the roughly 6-week temporal domain. The top table shows Monte Carlo estimates, which use the 80 ensemble members as independent samples and estimate the standard deviation from that. Each of the twin experiments uses the same 80 ensemble members as their prior means. The "Estimate" column is the expected value of the standard deviation given the sample, and the "95% CI" columns give uncertainty bounds on that uncertainty estimate. The point estimates should be the same down columns, with some deviations from sampling variability, and the confidence intervals should get narrower. The deterministic calculations use the reduced-resolution analysis covariance matrix, calculated in two different ways. The first does not attempt to account for aggregation error and uses Equation 5 to calculate the posterior variance, and the second attempts to do so using Equation 6 for the posterior variance. All of the reduced-resolution covariance matrices used to produce the results shown here have a temporal resolution of 7 days. The standard deviations reported in the "prior" column should be the same, with differences from sampling variability and from saving a coarser-resolution version of the full prior covariance matrix. The identical-twin posterior standard deviation estimates are estimating the same thing and are expected to be equal. The Monte Carlo and deterministic estimates of the posterior uncertainty in the fraternal-twin experiment measure different quantities and are not expected to be identical. In particular, the deterministic approximations to the prior and posterior uncertainties reflect only the assumptions of the inversion and would be the value reported by an inversion. The Monte Carlo estimate of the posterior uncertainty for the fraternal-twin experiment uses the same prior ensemble as the identical-twin experiment, which means the Monte Carlo estimate is related to the difference between the fraternal-twin posterior and the "truth".

For the identical-twin experiment, comparing the approximate analytic and Monte Carlo estimates of the standard deviation for the domain-average flux indicates the approximations used to compute and store the posterior covariance matrix at a computationally tractable resolution tend to make the narrowing of the posterior distribution relative to the prior around ten percent too large at the resolutions used here.

To be specific, the deterministic posterior estimates for the standard deviation of the domain-average flux in Table 1 lie below the 95% confidence intervals calculated for the stochastic estimates of the standard deviation in the same table (Oliphant, 2006a), so long as the confidence interval is based on more than five realizations of the prior noise. This mismatch is not simply an artifact of the different approaches used: The deterministic approximation for the prior variance, given in the same table, is well within the confidence interval for the stochastic approximation of that quantity. The deterministic approximations to both the prior and posterior standard deviation for the domain-average flux decrease with increasing resolution, becoming more confident in the average flux across the domain as the resolution of the uncertainty becomes coarser. This underestimate of the analytic covariance matrix is a potential concern for future inversion studies, though compared to the other assumptions made in an inversion, this may not be the dominant source of uncertainty in the posterior covariance estimates, especially when the resolution of the posterior covariance (Yadav & Michalak, 2013) is not much lower than that of the posterior mean estimates.

For the fraternal-twin experiment, attempting to account for the aggregation error produced a negative posterior error variance for the domain-average flux, but the posterior error variance for the domain-average flux calculated without an attempt to account for aggregation error is positive and is shown in Table 1. Note that the fraternal-twin OSSE uses the same 80 ensemble members for its ensemble mean estimates as the identical-twin OSSE, so the Monte Carlo estimates of the posterior uncertainty reflect the distribution of the posterior around the "truth," while the deterministic estimates of the posterior uncertainty are calculated using the assumptions of the fraternal-twin inversion, one of those assumptions being that the correlation length and time in the prior covariance of the fraternal-twin experiment are correct. The Monte Carlo estimates, on the other hand, use information outside of those assumptions, the 80 flux ensemble members generated a without using the prior covariance, to provide a more complete picture of the uncertainty and the difference between the fraternal-twin posteriors and the "truth." The factor-of-two discrepancy between the analytic and Monte-Carlo estimates of the uncertainty is rather larger than that in the identical-twin experiment, affirming that the correlation parameters are important to the posterior covariance and to the relationship between the posterior covariance and the difference between the posterior and the "truth."

The quality of the lower-resolution approximation to the posterior uncertainty does not appear to be very dependent on the resolution at which the posterior covariance is calculated if no attempt is made to account for aggregation error. If such an attempt is made following Equation 5, the quality of the approximation varies greatly depending on the spatial resolution, performing better than the direct approach when the resolution is higher than the correlation length chosen for the prior and worse when the resolution is coarser than the correlation length.

5. Conclusions

This study demonstrates a newly developed, high-resolution (27 km × 27 km in space, 6 hourly in time), continental-scale CO_2 surface flux inversion framework. The methodology presented here combines spatial and temporal error structures in an efficient mesoscale inversion system, allowing the system to solve for fluxes at these relatively high spatial and temporal resolutions, and avoiding the potential degradation in the accuracy of the inversion that can result from solving for fluxes at coarser resolution. When applied to real observations collected from 30 tower locations across North America, the combination of the Kronecker product implementation of Yadav and Michalak (2013) and spectral methods for the prior error correlations should significantly improve the resolution of inverse fluxes, which previous studies have indicated is important for the accuracy of inversion results (Ogle et al., 2015; Schuh et al., 2013). In addition, the ability to optimize multiple prior mean estimates at once will allow for uncertainty assessments using the Monte-Carlo approach of Michalak et al. (2004) and Bousserez et al. (2015), or the prior sensitivity approach of Lauvaux et al. (2012) using ensembles of prior mean estimates designed to reflect the full range of uncertainty in the fluxes, such as those provided by MsTMIP (Huntzinger et al., 2018) or the ACT-America CASA ensemble (Zhou et al., 2020).

The improved representation of the posterior uncertainty in the fraternal-twin OSSE using Monte Carlo methods rather than deterministic ones suggests that the generation of prior mean estimates using only noise realizations based upon the assumptions in the prior covariance limits the quality of the posterior flux estimates. The fraternal-twin OSSE results suggest that using ensemble members incorporating different vegetation models, different inputs for the vegetation models, and different downscaling of the models from monthly to hourly outputs would result in a more robust understanding of the the range of the uncertainty in the posterior fluxes.

The largest limitation of this approach is the assumption that the correlation length does not change over the domain. Previous studies have not found definite changes across a continent (Hilton et al., 2013; Kountouris et al., 2015) but have noted that there are differences between continents (Kountouris et al., 2015). Representing this variation in correlation length over space is not possible using spectral methods but can be done using wavelets (Deckmyn & Berre, 2005). Such an approach has been implemented for $ffCO_2$ inversions in Ray et al. (2013, 2014, 2015), but these methods have not yet been extended to biogenic CO_2 inversions.

The prior flux errors used in this paper confront the same problem described by Kountouris et al. (2015), which found that using correlation length and time scales taken from comparisons of eddy-covariance flux tower data to vegetation-model-predicted fluxes produced uncertainty estimates for continental-scale fluxes that were much lower than top-down uncertainty estimates from other studies. This study achieves continental-scale flux uncertainties in line with previous work at the cost of grid-point-level flux errors much higher than expected—for example, standard deviations in excess of 40 $\mu mol/(m^2 s)$ for much of the corn-growing regions of the Midwest (Figure 3). In contrast, Lokupitiya et al. (2009a) and DesJardins et al. (1984) indicate that around 40 $\mu mol/(m^2 s)$ is a good value for net ecosystem exchange (NEE) over growing corn during the day, while the standard deviation of the model-data difference under the same conditions is closer to 10 to 20 $\mu mol/(m^2 s)$ for a comparison of half-hourly fluxes from SiBcrop to AmeriFlux eddy-covariance data (Lokupitiya et al., 2009b). This inability to match both grid point variances and top-down continental uncertainty estimates seems to indicate the assumed correlation model is oversimplified and should be examined more carefully.

Appendix A: Code Location

The code used for the inversion is available under a three-clause BSD license (Morin et al., 2012) on GitHub (Blischak et al., 2016) through the PSU-inversion organization at https://github.com/psu-inversion/atmospheric-inverse-methods-for-flux-optimization and has also been archived at Zenodo (Wesloh, 2020). In particular, the scripts used are in the "paper2020" sub-directory: "make_noisy_fluxes.py" to generate the different realizations of the prior distribution for use as prior mean estimates in the OSSE, "month_inversion_magic_dask.py" to run the OSSE, "results_analysis.py" to generate the OSSE plots, and "plot_temporal covariances.py" to make Figure 4. Documentation for the inversion software described in this paper is available at https://psu-inversion.github.io/atmospheric-inverse-methods-for-flux-optimization. Wilson et al. (2014) note the importance of tests to ensure the reliability of software (Heroux & Willenbring, 2009; Heaton & Carver, 2015; Wilson, 2006); the tests for this package can be run from the root directory using tox or "python setup.py test".

The new LPDM postprocessing software, written in IDL and python, is available on GitHub through the PSU-Inversion organization at https://github.com/psu-inversion/LPDM-postprocessing or Wesloh & Lauvaux (2020) under a three-clause BSD license (Morin et al., 2012). The influence functions used in this study are made available through the PSU DataCommons (Wesloh & Lauvaux, 2019).

Acronyms

ABL	atmospheric boundary layer
ACT-America	Atmospheric Carbon and Transport–America
CMS	Carbon Monitoring System
FFT	fast Fourier transform (Cooley & Tukey, 1965)
FFTW	Fastest Fourier Transform in the West (Frigo & Johnson, 2005)
GMD	Global Monitoring Division
JPL	Jet Propulsion Laboratory
LPDM	Lagrangian particle dispersion model of Uliasz (1993, 1994).
NASA	National Aeronautics and Space Administration
NOAA	National Oceanic and Atmospheric Administration
OSSE	observing system simulation experiment (Errico & Privé, 2018)
TKE	turbulent kinetic energy
WRF	Weather Research and Forecast model (Skamarock et al., 2008)
WRF-Chem	Weather Research and Forecast–Chemistry (Grell et al., 2005)

Notation

A	analysis error covariance: uncertainty estimate in our posterior
B	background error covariance: uncertainty estimate in our prior
CO_2	carbon dioxide
H	influence function: derivative of observations with respect to sources
K	Kalman gain matrix: $K = BH^T\left(HBH^T + R\right)^{-1}$
$\mathcal{N}(\mu, \Sigma)$	the multivariate normal distribution with mean μ and covariance Σ
ppm	parts per million
R	observation error covariance: combines instrument uncertainty in observations and transport uncertainty in modeling how the fluxes impact the observations
$\boldsymbol{x}_a$	analysis estimate of the fluxes; taken from the mean of the posterior distribution
$\boldsymbol{x}_b$	background estimate of the fluxes; serves as the mean of the prior distribution
$\boldsymbol{x}_t$	the true fluxes; known for OSSE
y	observed mole fractions
C^T	the transpose of the real matrix C
C^{-1}	the inverse of the non-singular square matrix C
$\hat{C}(\nu)$	the Fourier transform of the function $C(t)$

Data Availability Statement

The WRF simulation is available at Lauvaux & Butler (2016). The baseline fluxes were obtained from the prior biological fluxes of CMS-Flux (Liu et al., 2014) and are available as NASA Carbon Monitoring System (2013).

Acknowledgments

Many thanks to Sha Feng and Klaus Keller for extensive feedback improving the focus and presentation of the figures. Plots were generated using Matplotlib, Cartopy, and XArray on Python 3.6.4, with coastlines and borders using Natural Earth data (Hoyer & Hamman, 2017; Hunter, 2007; Met Office, 2010; van Rossum, 1995). Extensive use was made of Numpy and Scipy for the low-level arithmetic and linear algebra and of FFTW via pyFFTW for Fourier transforms (Frigo & Johnson, 2018, 2005; Gomersall, 2016; Jones et al., 2001; Oliphant, 2006b; Virtanen et al., 2020). This work was funded by the NASA ACT-America project, the Gulf Coast Intensive (GCI) project, the Dr. Dennis W. and Dr. Joan S. Thomson Distinguished Graduate Fellowship, and the Anne C. Wilson Graduate Fellowship. ACT-America project is a NASA Earth Venture Suborbital 2 project funded by NASA's Earth Science Division, Grant NNX15AG76G to Penn State. The GCI was supported by NASA Terrestrial Carbon Cycle program, Grant NNX14AJ17G.

References

Agustí-Panareda, A., Diamantakis, M., Massart, S., Chevallier, F., Muñoz Sabater, J., Barré, J., et al. (2019). Modelling CO_2 weather—Why horizontal resolution matters. *Atmospheric Chemistry and Physics Discussions*, *2019*, 1–48. https://doi.org/10.5194/acp-2019-177

Anav, A., Friedlingstein, P., Beer, C., Ciais, P., Harper, A., Jones, C., et al. (2015). Spatiotemporal patterns of terrestrial gross primary production: A review. *Reviews of Geophysics*, *53*, 785–818. https://doi.org/10.1002/2015RG000483

Andres, R. J., Boden, T. A., & Higdon, D. (2014). A new evaluation of the uncertainty associated with CDIAC estimates of fossil fuel carbon dioxide emission. *Tellus B: Chemical and Physical Meteorology*, *66*(1), 23616. https://doi.org/10.3402/tellusb.v66.23616

Andrews, A. E., Kofler, J. D., Trudeau, M. E., Williams, J. C., Neff, D. H., Masarie, K. A., et al. (2014). CO_2, CO, and CH_4 measurements from tall towers in the NOAA Earth System Research Laboratory's global greenhouse gas reference network: Instrumentation, uncertainty analysis, and recommendations for future high-accuracy greenhouse gas monitoring efforts. *Atmospheric Measurement Techniques*, *7*(2), 647–687. https://doi.org/10.5194/amt-7-647-2014

Bakwin, P. S., Tans, P. P., Hurst, D. F., & Zhao, C. (1998). Measurements of carbon dioxide on very tall towers: Results of the NOAA/CMDL program. *Tellus B: Chemical and Physical Meteorology*, *50*(5), 401–415. https://doi.org/10.3402/tellusb.v50i5.16216

Bannister, R. N. (2008). A review of forecast error covariance statistics in atmospheric variational data assimilation. II: Modelling the forecast error covariance statistics. *Quarterly Journal of the Royal Meteorological Society*, *134*(637), 1971–1996. https://doi.org/10.1002/qj.340

Barnard, G. A., & Bayes, T. (1958). Studies in the history of probability and statistics: IX. Thomas Bayes's essay towards solving a problem in the doctrine of chances. *Biometrika*, *45*(3/4), 293–315. https://doi.org/10.2307/2333180

Battle, M., Bender, M. L., Tans, P. P., White, J. W. C., Ellis, J. T., Conway, T., & Francey, R. J. (2000). Global carbon sinks and their variability inferred from atmospheric O_2 and $\delta 13C$. *Science*, *287*(5462), 2467–2470. https://doi.org/10.1126/science.287.5462.2467

Bennett, A. F. (2002). *Inverse modeling of the ocean and atmosphere*. Cambridge: Cambridge University Press.

Blischak, J. D., Davenport, E. R., & Wilson, G. (2016). A quick introduction to version control with git and github. *PLOS Computational Biology*, *12*(1). https://doi.org/10.1371/journal.pcbi.1004668

Bocquet, M. (2005). Grid resolution dependence in the reconstruction of an atmospheric tracer source. *Nonlinear Processes in Geophysics*, *12*, 219–233. https://doi.org/10.5194/npg-12-219-2005

Bocquet, M., Wu, L., & Chevallier, F. (2011). Bayesian design of control space for optimal assimilation of observations. Part I: Consistent multiscale formalism. *Quarterly Journal of the Royal Meteorological Society*, *137*(658), 1340–1356. https://doi.org/10.1002/qj.837

Bousquet, P., Peylin, P., Ciais, P., Le Quéré, C., Friedlingstein, P., & Tans, P. P.(2000). Regional changes in carbon dioxide fluxes of land and oceans since 1980. *Science*, *290*(5495), 1342–1346. https://doi.org/10.1126/science.290.5495.1342

Bousserez, N., & Henze, D. K. (2018). Optimal and scalable methods to approximate the solutions of large-scale Bayesian problems: Theory and application to atmospheric inversion and data assimilation. *Quarterly Journal of the Royal Meteorological Society*, *144*(711), 365–390. https://doi.org/10.1002/qj.3209

Bousserez, N., Henze, D. K., Perkins, A., Bowman, K. W., Lee, M., Liu, J., et al. (2015). Improved analysis-error covariance matrix for high-dimensional variational inversions: Application to source estimation using a 3D atmospheric transport model. *Quarterly Journal of the Royal Meteorological Society*, *141*(690), 1906–1921. https://doi.org/10.1002/qj.2495

Butler, M. P., Lauvaux, T., Feng, S., Liu, J., Bowman, K. W., & Davis, K. J. (2020). Atmospheric simulations of total column CO_2 mole fractions from global to mesoscale within the carbon monitoring system flux inversion framework. *Atmosphere*, *11*(8), 787. https://doi.org/10.3390/atmos11080787

Chen, K. (2006). Lagrangian particle dispersion model (LPDM) technical description (U) (*US0605434*): USDOE. https://www.osti.gov/servlets/purl/891677

Chen, H. W., Zhang, F., Lauvaux, T., Davis, K. J., Feng, S., Butler, M. P., & Alley, R. B. (2019). Characterization of regional-scale CO_2 transport uncertainties in an ensemble with flow-dependent transport errors. *Geophysical Research Letters*, *46*, 4049–4058. https://doi.org/10.1029/2018GL081341

Chevallier, F., Viovy, N., Reichstein, M., & Ciais, P. (2006). On the assignment of prior errors in Bayesian inversions of CO_2 surface fluxes. *Geophysical Research Letters*, *33*, L13802. https://doi.org/10.1029/2006GL026496

Chevallier, F., Wang, T., Ciais, P., Maignan, F., Bocquet, M., Altaf Arain, M., et al. (2012). What eddy-covariance measurements tell us about prior land flux errors in CO_2-flux inversion schemes. *Global Biogeochemical Cycles*, *26*, GB1021. https://doi.org/10.1029/2010GB003974

Ciais, P., Rayner, P., Chevallier, F., Bousquet, P., Logan, M., Peylin, P., & Ramonet, M. (2010). Atmospheric inversions for estimating CO_2 fluxes: Methods and perspectives. *Climatic Change*, *103*(1-2), 69–92. https://doi.org/10.1007/s10584-010-9909-3

Cooley, J. W., & Tukey, J. W. (1965). An algorithm for the machine calculation of complex fourier series. *Mathematics of Computation*, *19*(90), 297–301. https://doi.org/10.2307/2003354

Díaz Isaac, L. I., Lauvaux, T., Davis, K. J., Miles, N. L., Richardson, S. J., Jacobson, A. R., & Andrews, A. E. (2014). Model-data comparison of MCI field campaign atmospheric CO_2 mole fractions. *Journal of Geophysical Research: Atmospheres*, *119*, 10,536–10,551. https://doi.org/10.1002/2014JD021593

Díaz-Isaac, L. I., Lauvaux, T., & Davis, K. J. (2018). Impact of physical parameterizations and initial conditions on simulated atmospheric transport and CO_2 mole fractions in the US Midwest. *Atmospheric Chemistry and Physics*, *18*(20), 14,813–14,835. https://doi.org/10.5194/acp-18-14813-2018

Daubechies, I. (1988). Orthonormal bases of compactly supported wavelets. *Communications on Pure and Applied Mathematics*, *41*(7), 909–996. https://doi.org/10.1002/cpa.3160410705

Davis, K. J., Bakwin, P. S., Yi, C., Berger, B. W., Zhao, C., Teclaw, R. M., & Isebrands, J. G. (2003). The annual cycles of CO_2 and H_2O exchange over a northern mixed forest as observed from a very tall tower. *Global Change Biology*, *9*(9), 1278–1293. https://doi.org/10.1046/j.1365-2486.2003.00672.x

Deckmyn, A., & Berre, L. (2005). A wavelet approach to representing background error covariances in a limited-area model. *Monthly Weather Review*, *133*(5), 1279–1294. https://doi.org/10.1175/MWR2929.1

DesJardins, R. L., Buckley, D. J., & Amour, G. S. (1984). Eddy flux measurements of CO_2 above corn using a microcomputer system. *Agricultural and Forest Meteorology*, *32*, 257–265. https://doi.org/10.1016/0168-1923(84)90053-4

Dietrich, C. R., & Newsam, G. N. (1993). A fast and exact method for multidimensional Gaussian stochastic simulations. *Water Resources Research*, *29*, 2861–2869. https://doi.org/10.1029/93WR01070

ESRL (2017). CarbonTracker-Lagrange. ESRL Global Monitoring Division—Global Greenhouse Gas Reference Network. https://www.esrl.noaa.gov/gmd/ccgg/carbontracker-lagrange/

Enting, I. G., & Mansbridge, J. V. (1989). Seasonal sources and sinks of atmospheric CO_2 direct inversion of filtered data. *Tellus B: Chemical and Physical Meteorology*, *41*(2), 111–126. https://doi.org/10.3402/tellusb.v41i2.15056

Errico, R. M., & Privé, N. C. (2018). Some general and fundamental requirements for designing observing system simulation experiments (OSSEs): World Meteorological Organization. https://www.wmo.int/pages/prog/arep/wwrp/new/documents/Final_WWRP_2018_8.pdf

Errico, R. M., Yang, R., Priv, N. C., Tai, K.-S., Todling, R., Sienkiewicz, M. E., & Guo, J. (2013). Development and validation of observing-system simulation experiments at NASA's Global Modeling and Assimilation Office. *Quarterly Journal of the Royal Meteorological Society*, *139*(674), 1162–1178. https://doi.org/10.1002/qj.2027

Fisher, J. B., Sikka, M., Huntzinger, D. N., Schwalm, C. R., Liu, J., Wei, Y., et al. (2016). CMS: Modeled net ecosystem exchange at 3-hourly time steps, 2004–2010. https://doi.org/10.3334/ORNLDAAC/1315

Friedlingstein, P., Meinshausen, M., Arora, V. K., Jones, C. D., Anav, A., Liddicoat, S. K., & Knutti, R.(2014). Uncertainties in CMIP5 climate projections due to carbon cycle feedbacks. *Journal of Climate*, *27*(2), 511–526. https://doi.org/10.1175/JCLI-D-12-00579.1

Frigo, M., & Johnson, S. G. (2005). The design and implementation of FFTW3. *Proceedings of the IEEE*, *93*(2), 216–231. https://doi.org/10.1109/JPROC.2004.840301

Frigo, M., & Johnson, S. G. (2018). FFTW home page. MIT, http://www.fftw.org/

Geels, C., Gloor, M., Ciais, P., Bousquet, P., Peylin, P., Vermeulen, A. T., et al. (2007). Comparing atmospheric transport models for future regional inversions over Europe—Part 1: Mapping the atmospheric CO_2 signals. *Atmospheric Chemistry and Physics*, *7*(13), 3461–3479. https://doi.org/10.5194/acp-7-3461-2007

Gentleman, W. M., & Sande, G. (1966). Fast Fourier transforms: For fun and profit. In *Proceedings of the November 7-10, 1966, fall joint computer conference*, *AFIPS '66 (Fall)* (pp. 563–578). New York, NY, USA: ACM. https://doi.org/10.1145/1464291.1464352

Gerbig, C., Lin, J. C., Wofsy, S. C., Daube, B. C., Andrews, A. E., Stephens, B. B., et al. (2003). Toward constraining regional-scale fluxes of CO_2 with atmospheric observations over a continent: 1. Observed spatial variability from airborne platforms. *Journal of Geophysical Research*, *108*, 4757. https://doi.org/10.1029/2003JD003770

Gomersall, H. (2016). pyFFTW documentation. pyFFTW developers, https://pyfftw.readthedocs.io/en/latest/

Gourdji, S. M., Mueller, K. L., Yadac, V., Huntzinger, D. N., Andrews, A. E., Trudeau, M., et al. (2012). North American CO_2 exchange: Inter-comparison of modeled estimates with results from a fine-scale atmospheric inversion. *Biogeosciences*, *9*, 457–475. https://doi.org/10.5194/bg-9-457-2012

Grell, G. A., Peckham, S. E., Schmitz, R., McKeen, S. A., Frost, G., Skamarock, W. C., & Eder, B. (2005). Fully coupled "online" chemistry within the WRF model. *Atmospheric Environment*, *39*(37), 6957–6975. https://doi.org/10.1016/j.atmosenv.2005.04.027

Gurney, K. R., Law, R. M., Denning, A. S., Rayner, P. J., Baker, D., Bousquet, P., et al. (2003). Transcom 3 CO_2 inversion intercomparison: 1. Annual mean control results and sensitivity to transport and prior flux information. *Tellus B*, *55*(2), 555–579. https://doi.org/10.1034/j.1600-0889.2003.00049.x

Gurney, K. R., Law, R. M., Denning, A. S., Rayner, P. J., Baker, D., Bousquet, P., et al. (2002). Towards robust regional estimates of CO_2 sources and sinks using atmospheric transport models. *Nature*, *415*(6872), 626–630. https://doi.org/10.1038/415626a

Hayes, D. J., Turner, D. P., Stinson, G., McGuire, A. D., Wei, Y., West, T. O., et al. (2012). Reconciling estimates of the contemporary North American carbon balance among terrestrial biosphere models, atmospheric inversions, and a new approach for estimating net ecosystem exchange from inventory-based data. *Global Change Biology*, *18*(4), 1282–1299. https://doi.org/10.1111/j.1365-2486.2011.02627.x

Heaton, D., & Carver, J. C. (2015). Claims about the use of software engineering practices in science: A systematic literature review. *Information and Software Technology*, *67*, 207–219. https://doi.org/10.1016/j.infsof.2015.07.011

Heroux, M. A., & Willenbring, J. M. (2009). Barely sufficient software engineering: 10 practices to improve your CSE software. In *2009 ICSE Workshop on Software Engineering for Computational Science and Engineering*(pp. 15–21) https://ieeexplore.ieee.org/document/5069157

Hilton, T. W., Davis, K. J., Keller, K., & Urban, N. M. (2013). Improving North American terrestrial CO_2 flux diagnosis using spatial structure in land surface model residuals. *Biogeosciences*, *10*(7), 4607–4625. https://doi.org/10.5194/bg-10-4607-2013

Hotelling, H. (1933). Analysis of a complex of statistical variables into principal components. *Journal of Educational Psychology*, *24*, 417–441. https://doi.org/10.1037/h0071325

Houghton, R. A., House, J. I., Pongratz, J., van der Werf, G. R., DeFries, R. S., Hansen, M. C., et al. (2012). Carbon emissions from land use and land-cover change. *Biogeosciences*, *9*(12), 5125–5142. https://doi.org/10.5194/bg-9-5125-2012

Houtekamer, P. L., Lefaivre, L., Derome, J., Ritchie, H., & Mitchell, H. L. (1996). A system simulation approach to ensemble prediction. *Monthly Weather Review*, *124*(6), 1225–1242. https://doi.org/10.1175/1520-0493(1996)124<1225:ASSATE>2.0.CO;2

Hoyer, S., & Hamman, J. (2017). xarray: N-D labeled arrays and datasets in Python. *Journal of Open Research Software*, *5*(1), 10. https://doi.org/10.5334/jors.148/

Hu, L., Andrews, A. E., Thoning, K. W., Sweeney, C., Miller, J. B., Michalak, A. M., et al. (2019). Enhanced North American carbon uptake associated with El Niño. *Science Advances*, *5*(6), eaaw0076. https://doi.org/10.1126/sciadv.aaw0076

Hunter, J. D. (2007). Matplotlib: A 2D graphics environment. *Computing In Science & Engineering*, *9*(3), 90–95. https://doi.org/10.1109/MCSE.2007.55

Huntzinger, D. N., Gourdji, S. M., Mueller, K. L., & Michalak, A. M. (2011). A systematic approach for comparing modeled biospheric carbon fluxes across regional scales. *Biogeosciences*, *8*(6), 1579–1593. https://doi.org/10.5194/bg-8-1579-2011

Huntzinger, D. N., Michalak, A. M., Schwalm, C., Ciais, P., King, A. W., Fang, Y., et al. (2017). Uncertainty in the response of terrestrial carbon sink to environmental drivers undermines carbon-climate feedback predictions. *Scientific Reports*, *7*(1), 4765. https://doi.org/10.1038/s41598-017-03818-2

Huntzinger, D. N., Post, W. M., Wei, Y., Michalak, A. M., West, T. O., Jacobson, A. R., et al. (2012). North American Carbon Program (NACP) regional interim synthesis: Terrestrial biospheric model intercomparison. *Ecological Modelling*, *232*, 144–157. https://doi.org/10.1002/qj.3209

Huntzinger, D. N., Schwalm, C. R., Wei, Y., Cook, R. B., Michalak, A. M., Schaefer, K., et al. (2018). NACP MsTMIP: Global 0.5-degree model outputs in standard format, version 1.0. ORNL Distributed Active Archive Center, https://doi.org/10.3334/ORNLDAAC/1338

Ide, K., Courtier, P., Ghil, M., & Lorenc, A. C. (1997). Unified notation for data assimilation: Operational, sequential and variational. *Journal of the Meteorological Society of Japan. Series II*, *75*(1B), 181–189. https://doi.org/10.2151/jmsj1965.75.1B_181

Jacobson, A. R., & Miller, J. B. (2018). Observations of atmospheric carbon dioxide and methane: A sustained assessment report. In N. Cavallaro, et al. (Eds.), *Second state of the carbon cycle report (SOCCR2): A sustained assessment report* (pp. 337–364). Washington, DC: U. S. Global Change Research Program. https://carbon2018.globalchange.gov/chapter/8/

Jones, E., Oliphant, T., Peterson, P., et al. (2001). SciPy: Open source scientific tools for Python. http://www.scipy.org/

Kaminski, T., Rayner, P. J., Heimann, M., & Enting, I. G. (2001). On aggregation errors in atmospheric transport inversions. *Journal of Geophysical Research*, *106*(D5), 4703–4715. https://doi.org/10.1029/2000JD900581

Karion, A., Lauvaux, T., Lopez Coto, I., Sweeney, C., Mueller, K., Gourdji, S., et al. (2019). Intercomparison of atmospheric trace gas dispersion models: Barnett shale case study. *Atmospheric Chemistry and Physics*, *19*(4), 2561–2576. https://doi.org/10.5194/acp-19-2561-2019

King, A. W., Andres, R. J., Davis, K. J., Hafer, M., Hayes, D. J., Huntzinger, D. N., et al. (2015). North America's net terrestrial CO_2 exchange with the atmosphere 1990–2009. *Biogeosciences*, *12*(2), 399–414. https://doi.org/10.5194/bg-12-399-2015

Kountouris, P., Gerbig, C., Rödenbeck, C., Karstens, U., Koch, T. F., & Heimann, M. (2018a). Atmospheric CO_2 inversions on the mesoscale using data-driven prior uncertainties: Quantification of the European terrestrial CO_2 fluxes. *Atmospheric Chemistry and Physics*, *18*(4), 3047–3064. https://doi.org/10.5194/acp-18-3047-2018

Kountouris, P., Gerbig, C., Rödenbeck, C., Karstens, U., Koch, T. F., & Heimann, M. (2018b). Technical note: Atmospheric CO_2 inversions on the mesoscale using data-driven prior uncertainties: Methodology and system evaluation. *Atmospheric Chemistry and Physics*, *18*(4), 3027–3045. https://doi.org/10.5194/acp-18-3027-2018

Kountouris, P., Gerbig, C., Totsche, K.-U., Dolman, A. J., Meesters, A. G. C. A., Broquet, G., et al. (2015). An objective prior error quantification for regional atmospheric inverse applications. *Biogeosciences*, *12*(24), 7403–7421. https://doi.org/10.5194/bg-12-7403-2015

Lauvaux, T., & Butler, M. (2016). CMS: Hourly carbon dioxide estimated using the WRF model, North America, 2010. ORNL Distributed Active Archive Center, ORNL DAAC. https://doi.org/10.3334/ORNLDAAC/1338

Lauvaux, T., & Davis, K. J. (2014). Planetary boundary layer errors in mesoscale inversions of column-integrated CO_2 measurements. *Journal of Geophysical Research: Atmospheres*, *119*, 490–508. https://doi.org/10.1002/2013JD020175

Lauvaux, T., Miles, N. L., Deng, A., Richardson, S. J., Cambaliza, M. O., Davis, K. J., et al. (2016). High-resolution atmospheric inversion of urban CO2 emissions during the dormant season of the Indianapolis flux experiment (influx). *Journal of Geophysical Research: Atmospheres*, *121*(10), 5213–5236. https://doi.org/10.1002/2015JD024473

Lauvaux, T., Pannekoucke, O., Sarrat, C., Chevallier, F., Ciais, P., Noilhan, J., & Rayner, P. J. (2009). Structure of the transport uncertainty in mesoscale inversions of CO_2 sources and sinks using ensemble model simulations. *Biogeosciences*, *6*(6), 1089–1102. https://doi.org/10.5194/bg-6-1089-2009

Lauvaux, T., Schuh, A., Bocquet, M., Wu, L., Richardson, S., Miles, N., & Davis, K. (2012). Network design for mesoscale inversions of CO_2 sources and sinks. *Tellus B*, *64*, 17980. https://doi.org/10.3402/tellusb.v64i0.17980

Lauvaux, T., Schuh, A., Uliasz, M., Richardson, S., Miles, N., Andrews, A., et al. (2012). Constraining the CO_2 budget of the corn belt: Exploring uncertainties from the assumptions in a mesoscale inverse system. *Atmospheric Chemistry and Physics*, *12*(1), 337–354. https://doi.org/10.5194/acp-12-337-2012

Law, R. M., Rayner, P. J., Steele, L. P., & Enting, I. G. (2002). Using high temporal frequency data for CO_2 inversions. *Global Biogeochemical Cycles*, *16*(4), 1–1–1–18. https://doi.org/10.1029/2001GB001593

Law, R. M., Rayner, P. J., Steele, L. P., & Enting, I. G. (2003). Data and modelling requirements for CO_2 inversions using high-frequency data. *Tellus: Series B*, *55*(2), 512–521. https://doi.org/10.1034/j.1600-0889.2003.00029.x

Le Quéré, C., Andrew, R. M., Canadell, J. G., Sitch, S., Korsbakken, J. I., Peters, G. P., et al. (2016). Global carbon budget 2016. *Earth System Science Data*, *8*(2), 605–649. https://doi.org/10.5194/essd-8-605-2016

Le Quéré, C., Andrew, R. M., Friedlingstein, P., Sitch, S., Pongratz, J., Manning, A. C., et al. (2018). Global carbon budget 2017. *Earth System Science Data*, *10*(1), 405–448. https://doi.org/10.5194/essd-10-405-2018

Liu, J., Bowman, K. W., Lee, M., Henze, D. K., Bousserez, N., Brix, H., et al. (2014). Carbon monitoring system flux estimation and attribution: Impact of ACOS-GOSAT XCO_2 sampling on the inference of terrestrial biospheric sources and sinks. *Tellus B: Chemical and Physical Meteorology*, *66*(1), 22486. https://doi.org/10.3402/tellusb.v66.22486

Lokupitiya, E., Denning, S., Paustian, K., Baker, I., Schaefer, K., Verma, S., et al. (2009a). Incorporation of crop phenology in simple biosphere model (SiBcrop) to improve land-atmosphere carbon exchanges from croplands. *Biogeosciences*, *6*(6), 969–986. https://doi.org/10.5194/bg-6-969-2009

Lokupitiya, E., Denning, S., Paustian, K., Baker, I., Schaefer, K., Verma, S., et al. (2009b). Corrigendum to "Incorporation of crop phenology in simple biosphere model (SiBcrop) to improve land-atmosphere carbon exchanges from croplands" published in Biogeosciences, 6, 969–986, 2009. *Biogeosciences*, *6*(6), 1103–1103. https://doi.org/10.5194/bg-6-1103-2009

Lorenc, A. C. (1988). Optimal nonlinear objective analysis. *Quarterly Journal of the Royal Meteorological Society*, *114*(479), 205–240. https://doi.org/10.1002/qj.49711447911

Lorenz, E. N. (1956). Empirical orthogonal functions and statistical weather prediction (*1*): Massachusetts Institute of Technology. http://eaps4.mit.edu/research/Lorenz/Empirical_Orthogonal_Functions_1956.pdf

Mallat, S. G. (1989). A theory for multiresolution signal decomposition: The wavelet representation. *IEEE Transactions on Pattern Analysis and Machine Intelligence*, *11*(7), 674–693. https://doi.org/10.1109/34.192463

Mellor, G. L., & Yamada, T. (1982). Development of a turbulence closure model for geophysical fluid problems. *Reviews of Geophysics*, *20*(4), 851–875. https://doi.org/10.1029/rg020i004p00851

Met Office (2010). Cartopy: A cartographic python library with a Matplotlib interface. http://scitools.org.uk/cartopy

Michalak, A. M., Bruhwiler, L., & Tans, P. P. (2004). A geostatistical approach to surface flux estimation of atmospheric trace gases. *Journal of Geophysical Research*, *109*, D14109. https://doi.org/10.1029/2003JD004422

Morin, A., Urban, J., & Sliz, P. (2012). A quick guide to software licensing for the scientist-programmer. *PLOS Computational Biology*, *8*(7), 1–7. https://doi.org/10.1371/journal.pcbi.1002598

NASA Carbon Monitoring System (2013). Top-down CO_2 attribution. NASA Jet Propulsion Laboratory, https://cmsflux.jpl.nasa.gov/DS-Attribution.aspx

NIST Digital Library of Mathematical Functions (2019). Release 1.0.24 of 2019-09-15. Retrieved 2019-11-20 from https://dlmf.nist.gov/1.14#E5, F. W. J. Olver, A. B. Olde Daalhuis, D. W. Lozier, B. I. Schneider, R. F. Boisvert, C. W. Clark, B. R. Miller, B. V. Saunders, H. S. Cohl, and M. A. McClain (eds.).

Normile, C., & Davis, K. J. (2017). Assessment of uncertainties in atmospheric transport and surface flux of carbon from the North American terrestrial biosphere (Ph.D. Thesis), The Pennsylvania State University.

Nowak, W., & Litvinenko, A. (2013). Kriging and Spatial Design Accelerated by Orders of Magnitude: Combining Low-Rank Covariance Approximations with FFT-Techniques. *Mathematical Geosciences*, *45*(4), 411–435. https://doi.org/10.1007/s11004-013-9453-6

Nowak, W., Tenkleve, S., Cirpka, O. A. (2003). Efficient computation of linearized cross-covariance and auto-covariance matrices of interdependent quantities. *Mathematical Geology*, *35*(1), 53–66. https://doi.org/10.1023/a:1022365112368

Ogle, S. M., Davis, K., Lauvaux, T., Schuh, A., Cooley, D., West, T. O., et al. (2015). An approach for verifying biogenic greenhouse gas emissions inventories with atmospheric CO_2 concentration data. *Environmental Research Letters*, *10*(3), 034012. https://doi.org/10.1088/1748-9326/10/3/034012/meta

Oliphant, T. E. (2006a). A Bayesian perspective on estimating mean, variance, and standard-deviation from data. Faculty Publications. Retrieved from https://scholarsarchive.byu.edu/facpub/278/

Oliphant, T. E. (2006b). A guide to NumPy. Trelgol Publishing.

Pacala, S. W., Hurtt, G. C., Baker, D., Peylin, P., Houghton, R. A., Birdsey, R. A., et al. (2001). Consistent land- and atmosphere-based U.S. carbon sink estimates. *Science*, *292*(5525), 2316–2320. https://doi.org/10.1126/science.1057320

Patra, P. K., Law, R. M., Peters, W., Rdenbeck, C., Takigawa, M., Aulagnier, C., et al. (2008). Transcom model simulations of hourly atmospheric CO_2: Analysis of synoptic-scale variations for the period 2002–2003. *Global Biogeochemical Cycles*, *22*, GB4013. https://doi.org/10.1029/2007GB003081

Pearson, K. (1901). LIII. On lines and planes of closest fit to systems of points in space. *The London, Edinburgh, and Dublin Philosophical Magazine and Journal of Science*, *2*(11), 559–572. https://doi.org/10.1080/14786440109462720

Peters, W., Jacobson, A. R., Sweeney, C., Andrews, A. E., Conway, T. J., Masarie, K., et al. (2007). An atmospheric perspective on North American carbon dioxide exchange: CarbonTracker. *Proceedings of the National Academy of Sciences*, *104*(48), 18,925–18,930. https://doi.org/10.1073/pnas.0708986104

Peylin, P., Baker, D., Sarmiento, J., Ciais, P., & Bousquet, P.(2002). Influence of transport uncertainty on annual mean and seasonal inversions of atmospheric CO_2 data. *Journal of Geophysical Research*, *107*(D19), ACH 5–1–ACH 5–25. https://doi.org/10.1029/2001JD000857

Peylin, P., Law, R. M., Gurney, K. R., Chevallier, F., Jacobson, A. R., Maki, T., et al. (2013). Global atmospheric carbon budget: results from an ensemble of atmospheric CO_2 inversions. *Biogeosciences*, *10*(10), 6699–6720. https://doi.org/10.5194/bg-10-6699-2013

Potempski, S., Galmarini, S., Addis, R., Astrup, P., Bader, S., Bellasio, R., et al. (2008). Multi-model ensemble analysis of the ETEX-2 experiment. *Atmospheric Environment*, *42*(31), 7250–7265. https://doi.org/10.1016/j.atmosenv.2008.07.027

Privé, N. C., & Errico, R. M. (2013). The role of model and initial condition error in numerical weather forecasting investigated with an observing system simulation experiment. *Tellus A: Dynamic Meteorology and Oceanography*, *65*(1). https://doi.org/10.3402/tellusa.v65i0.21740

Raczka, B. M., Davis, K. J., Huntzinger, D., Neilson, R. P., Poulter, B., Richardson, A. D., et al. (2013). Evaluation of continental carbon cycle simulations with North American flux tower observations. *Ecological Monographs*, *83*(4), 531–556. https://doi.org/10.1890/12-0893.1

Ray, J., Lee, J., Yadav, V., Lefantzi, S., Michalak, A. M., & van Bloemen Waanders, B. (2015). A sparse reconstruction method for the estimation of multi-resolution emission fields via atmospheric inversion. *Geoscientific Model Development*, *8*(4), 1259–1273. https://doi.org/10.5194/gmd-8-1259-2015

Ray, J., Yadav, V., Lee, J., Michalak, A. M., Lefantzi, S., van Bloemen Waanders, B., & McKenna, S. A.(2013). A multiresolution spatial parametrization for the estimation of fossil-fuel carbon dioxide emissions via atmospheric inversions: Sandia National Laboratories. https://www.sandia.gov/~jairay/Presentations/sand2013-2919.pdf

Ray, J., Yadav, V., Michalak, A. M., van Bloemen Waanders, B., & McKenna, S. A. (2014). A multiresolution spatial parameterization for the estimation of fossil-fuel carbon dioxide emissions via atmospheric inversions. *Geoscientific Model Development*, *7*(5), 1901–1918. https://doi.org/10.5194/gmd-7-1901-2014

Ryu, Y., Berry, J. A., & Baldocchi, D. D. (2019). What is global photosynthesis? History, uncertainties and opportunities. *Remote Sensing of Environment*, *223*, 95–114. https://doi.org/10.1016/j.rse.2019.01.016

Schimel, D., Stephens, B. B., & Fisher, J. B. (2015). Effect of increasing CO_2 on the terrestrial carbon cycle. *Proceedings of the National Academy of Sciences*, *112*(2), 436–441. https://doi.org/10.1073/pnas.1407302112

Schuh, A. E., Lauvaux, T., West, T. O., Denning, A. S., Davis, K. J., Miles, N., et al. (2013). Evaluating atmospheric CO_2 inversions at multiple scales over a highly inventoried agricultural landscape. *Global Change Biology*, *19*(5), 1424–1439. https://doi.org/10.1111/gcb.12141

Schwalm, C. R., Williams, C. A., Schaefer, K., Anderson, R., Arain, M. A., Baker, I., et al. (2010). A model-data intercomparison of CO_2 exchange across North America: Results from the North American Carbon Program site synthesis. *Journal of Geophysical Research*, *115*, G00H05. https://doi.org/10.1029/2009JG001229

Seibert, P., & Frank, A. (2004). Source-receptor matrix calculation with a lagrangian particle dispersion model in backward mode. *Atmospheric Chemistry and Physics*, *4*(1), 51–63. https://doi.org/10.5194/acp-4-51-2004

Skamarock, W. C., Klemp, J. B., Dudhia, J., Gill, D. O., Barker, D., Duda, M. G., et al. (2008). A description of the Advanced Research WRF version 3 (*475-STR*): NCAR. https://doi.org/10.5065/D68S4MVH

Stockham, T. G. (1966). High-speed convolution and correlation. In *Proceedings of the April 26-28, 1966, Spring Joint Computer Conference*, *AFIPS '66 (Spring)* (pp. 229–233). New York, NY, USA: ACM. https://doi.org/10.1145/1464182.1464209

Tans, P. P., Fung, I. Y., & Takahashi, T. (1990). Observational constraints on the global atmospheric CO_2 budget. *Science*, *247*(4949), 1431–1438. https://doi.org/10.1126/science.247.4949.1431

Tarantola, A. (2005). *Inverse problem theory and methods for model parameter estimation*, *Other Titles in Applied Mathematics*. Burlington, MA: Society for Industrial and Applied Mathematics. https://doi.org/10.1137/1.9780898717921

Torrence, C., & Compo, G. P. (1998). A practical guide to wavelet analysis. *Bulletin of the American Meteorological Society*, *79*(1), 61–78. https://doi.org/10.1175/1520-0477(1998)079<0061:APGTWA>2.0.CO;2

Uliasz, M. (1993). The atmospheric mesoscale dispersion modeling system. *Journal of Applied Meteorology*, *32*(1), 139–149. https://doi.org/10.1175/1520-0450(1993)032<0139:TAMDMS>2.0.CO:2

Uliasz, M. (1994). Lagrangian particle dispersion modeling in mesoscale applications. *Environ Model: Comput Methods and Softw for Simulat Environ Pollut and Its Adverse Effects (CMP)*, *2*, 71–102. http://indico.ictp.it/event/a02274/contribution/22/material/0/0.pdf

van Rossum, G. (1995). Python tutorial: Centrum voor Wiskunde en Informatica. https://ir.cwi.nl/pub/5007/05007D.pdf

Virtanen, P., Gommers, R., Oliphant, T. E., Haberland, M., Reddy, T., Cournapeau, D., et al. (2020). SciPy 1.0: Fundamental algorithms for scientific computing in Python. *Nature Methods*, *17*(3), 261–272. https://doi.org/10.1038/s41592-019-0686-2

Wesloh, D. (2020). Atmospheric Inverse Methods for Flux Optimization. *Zenodo*. https://doi.org/10.5281/zenodo.3966521

Wesloh, D., & Lauvaux, T. (2019). Gridded influence functions for NOAA tall towers for January 2010. Pennsylvania State University DataCommons. https://doi.org/10.26208/fh29-0y91

Wesloh, D., & Lauvaux, T. (2020). psu-inversion/LPDM-postprocessing: First release of PSU code related to Uliasz's LPDM. *Zenodo*. https://zenodo.org/record/3967222, https://doi.org/10.5281/zenodo.3967222

Wessman, C. A. (1992). Spatial scales and global change: Bridging the gap from plots to GCM grid cells. *Annual Review of Ecology and Systematics*, *23*, 175–200. http://www.jstor.org/stable/2097286

Wilson, G. (2006). Software carpentry: Getting scientists to write better code by making them more productive. *Computing in Science Engineering*, *8*(6), 66–69. https://doi.org/10.1109/MCSE.2006.122

Wilson, G., Aruliah, D. A., Brown, C. T., Chue Hong, N. P., Davis, M., Guy, R. T., et al. (2014). Best practices for scientific computing. *PLOS Biology*, *12*(1), 1–7. https://doi.org/10.1371/journal.pbio.1001745

Wu, L., Bocquet, M., Chevallier, F., Lauvaux, T., & Davis, K. (2013). Hyperparameter estimation for uncertainty quantification in mesoscale carbon dioxide inversions. *Tellus B: Chemical and Physical Meteorology*, *65*(1), 20,894–20,908. https://doi.org/10.3402/tellusb.v65i0.20894

Yadav, V., & Michalak, A. M. (2013). Improving computational efficiency in large linear inverse problems: An example from carbon dioxide flux estimation. *Geoscientific Model Development*, *6*(3), 583–590. https://doi.org/10.5194/gmd-6-583-2013

Zhao, M., Running, S. W., & Nemani, R. R. (2006). Sensitivity of Moderate Resolution Imaging Spectroradiometer (MODIS) terrestrial primary production to the accuracy of meteorological reanalyses. *Journal of Geophysical Research*, *111*, G01002. https://doi.org/10.1029/2004JG000004

Zhou, Y., Williams, C. A., Lauvaux, T., Davis, K. J., Feng, S., Baker, I., et al. (2020). A multi-year gridded data ensemble of surface biogenic carbon fluxes for North America: Evaluation and analysis of results. *Journal of Geophysical Research: Biogeosciences*, *125*, e2019JG005314. https://doi.org/10.1029/2019JG005314

Zhuravlev, R. V., Ganshin, A. V., Maksyutov, S. S., Oshchepkov, S. L., & Khattatov, B. V. (2013). Estimation of global CO_2 fluxes using ground-based and satellite (GOSAT) observation data with empirical orthogonal functions. *Atmospheric and Oceanic Optics*, *26*(6), 507–516. https://doi.org/10.1134/S1024856013060158

Zhuravlev, R. V., Khattatov, B., Kiryushov, B., & Maksyutov, S. (2011). Technical note: A novel approach to estimation of time-variable surface sources and sinks of carbon dioxide using empirical orthogonal functions and the Kalman filter. *Atmospheric Chemistry and Physics*, *11*(20), 10,305–10,315. https://doi.org/10.5194/acp-11-10305-2011